Novel Magnetically Separable Mesoporous Fe_2O_3@SBA-15 Nanocomposite with Fully Open Mesochannels for Protein Immobilization

Hsing-An Lin,[†] Chun-Hsia Liu,[†] Wei-Chia Huang,[†] Sz-Chian Liou,[‡] Ming-Wen Chu,[‡] Cheng-Hsuan Chen,[‡] Jyh-Fu Lee,[§] and Chia-Min Yang*,[†]

Department of Chemistry, National Tsing Hua University, Hsinchu 30013, Taiwan, Center for Condensed Matter Sciences, National Taiwan University, Taipei 10617, Taiwan, and National Synchrotron Radiation Research Center, Hsinchu 30076, Taiwan

Received February 26, 2008. Revised Manuscript Received June 24, 2008

Magnetically separable Fe_2O_3@SBA-15 nanocomposite with fully open mesochannels and bifunctional surface properties was prepared by selective deposition of iron oxide nanoparticles in the micropores of mesoporous SBA-15 silica with hydrophobic mesopore surface. The iron oxide nanoparticles embedded in the micropores were estimated to be composed of 67% α-Fe_2O_3 and 33% γ-Fe_2O_3, and the nanocomposite was found to exhibit superparamagnetic properties. With the bifunctional surface properties, the Fe_2O_3@SBA-15 nanocomposite showed enhanced adsorption capacity for cytochrome c and a maximum saturated uptake at neutral solution pH.

Introduction

Ordered mesoporous silica materials[1−4] are one of the most important scaffolds for constructing advanced nanocomposites on the nanometer scale.[4,5] For example, proteins or enzymes have been immobilized in mesoporous silicas for biotechnological applications, with the aims to improve the chemical/thermal stability of the biomolecules and to overcome the difficulties associated with their recovery and recycling.[6] Mesoporous SBA-15 silica[3] with hexagonally arranged channel-type (5−30 nm in diameter) mesopores are promising supports to immobilize proteins of small to medium size.[6a,7] In addition to the primary mesochannels, SBA-15 generally possesses microporosity in the silica walls originating from the occlusion of the EO chains of the structure-directing agent (Pluronic P-123, $EO_{20}PO_{70}EO_{20}$) during the synthesis.[8] On the other hand, magnetic materials are also attractive supports for protein immobilization,[9] for which the recovery and separation can be easily accomplished by using a magnet.

Aiming to combine the advantages of both types of materials, we herein report a novel magnetically separable Fe_2O_3@SBA-15 nanocomposite with fully open mesochannels and unique surface properties for protein immobilization. The preparation makes use of the bimodal pore system of SBA-15 silica and applies the method of selective surface functionalization we developed recently,[10] as depicted in

* Corresponding author. Fax: 886-3-5165521. Tel: 886-3-5731282. E-mail: cmyang@mx.nthu.edu.tw.
[†] National Tsing Hua University.
[‡] National Taiwan University.
[§] National Synchrotron Radiation Research Center.

(1) (a) Kresge, C. T.; Leonowicz, M. E.; Roth, W. J.; Vartuli, J. C.; Beck, J. S. *Nature* **1992**, *359*, 710. (b) Beck, J. S.; Vartuli, J. C.; Roth, W. J.; Leonowicz, M. E.; Kresge, C. T.; Schimitt, K. T.; Chu, C. T.-W.; Olson, D. H.; Sheppard, E. W.; McCullen, S. B.; Higgins, J. B.; Schlenker, J. L. *J. Am. Chem. Soc.* **1992**, *114*, 10834.
(2) (a) Yanagisawa, T.; Shimizu, T.; Kuroda, K.; Kato, C. *Bull. Chem. Soc. Jpn.* **1990**, *63*, 988. (b) Inagaki, S.; Fukushima, Y.; Kuroda, K *J. Chem. Soc., Chem. Commun.* **1993**, 680.
(3) (a) Zhao, D.; Feng, J.; Huo, Q.; Melosh, N.; Fredrickson, G. H.; Chmelka, B. F.; Stucky, G. D. *Science* **1998**, *279*, 548. (b) Zhao, D.; Huo, Q.; Feng, J.; Chmelka, B. F.; Stucky, G. D. *J. Am. Chem. Soc.* **1998**, *120*, 6024.
(4) (a) Ying, J. Y.; Mehnert, C. P.; Wong, M. S. *Angew. Chem., Int. Ed.* **1999**, *38*, 56. (b) Ciesla, U.; Schüth, F. *Microporous Mesoporous Mater.* **1999**, *27*, 131. (c) Sayari, A.; Hamoudi, S. *Chem. Mater.* **2001**, *13*, 3151. (d) de A. A.; Soler-Illia, G. J.; Sanchez, C.; Lebeau, B.; Patarin, J *Chem. Rev.* **2002**, *102*, 4093.
(5) (a) Moller, K.; Bein, T. *Chem. Mater.* **1998**, *10*, 2950. (b) Zhang, L.; Papaefthymiou, G. C.; Ying, J. Y. *J. Phys. Chem. B* **2001**, *105*, 7414. (c) Mumar, R.; Chen, H. T.; Escoto, J. L. V.; Lin, V. S. Y.; Pruski, M. *Chem. Mater.* **2006**, *18*, 4319.
(6) (a) Yiu, H. H. P.; Wright, P. A. *J. Mater. Chem.* **2005**, *15*, 3960. (b) Langer, R. *Nature* **1998**, *392*, 5. (c) Prata-Vidal, M.; Bouhallab, S.; Henry, G.; Aimar, P. *Biochem. Eng.* **2001**, *8*, 195. (d) Ahuja, S. K.; Ferreira, G. M.; Moreira, A. R. *Crit. Rev. Biotechnol.* **2004**, *24*, 125.
(7) (a) Han, Y. J.; Stucky, G. D.; Butler, A. *J. Am. Chem. Soc.* **1999**, *121*, 9897. (b) Washmon-Kriel, L.; Jimenez, V. L.; Balkus, K. J., Jr *J. Mol. Catal. B: Enzym.* **2000**, *10*, 453. (c) Takahashi, H.; Li, B.; Sasaki, T.; Miyazaki, C.; Kajino, T.; Inagaki, S. *Chem. Mater.* **2000**, *12*, 3301. (d) Lei, C.; Shin, Y.; Liu, J.; Ankerman, E. J. *J. Am. Chem. Soc.* **2000**, *124*, 11242.
(8) (a) Ryoo, R.; Ko, C. H.; Kruk, M.; Antochshuk, V.; Jaroniec, M. *J. Phys. Chem. B* **2000**, *104*, 11465. (b) Impéror-Clerc, M.; Davidson, P.; Davidson, A. *J. Am. Chem. Soc.* **2000**, *122*, 11925. (c) Ravikovitch, P. I.; Neimark, A. V. *J. Phys. Chem. B* **2001**, *105*, 6817. (d) Galarneau, A.; Cambon, H.; Di Renzo, F.; Ryoo, R.; Choi, M.; Fajula, F. *New J. Chem.* **2003**, *27*, 73.
(9) (a) Dyal, A.; Loos, K.; Noto, M.; Chang, S. W.; Spagnoli, C.; Shafi, K. V. P. M.; Ulman, A.; Cowman, M.; Gross, R. A. *J. Am. Chem. Soc.* **2003**, *125*, 1684. (b) Kim, J.; Lee, J.; Na, H. B.; Kim, B. C.; Youn, J. K.; Kwak, J. H.; Moon, K.; Lee, E.; Kim, J.; Park, J.; Dohnalkova, A.; Park, H. G.; Gu, M. B.; Chang, H. N.; Grate, J. W.; Hyeon, T. *Small* **2005**, *1*, 1203. (c) Eggleston, C. M.; Khare, N.; Lovelace, D. M. *J. Electron Spectrosc. Relat. Phenom.* **2006**, *150*, 220.
(10) (a) Yang, C. M.; Zibrowius, B.; Schmidt, W.; Schüth, F. *Chem. Mater.* **2003**, *15*, 3739. (b) Yang, C. M.; Zibrowius, B.; Schmidt, W.; Schüth, F. *Chem. Mater.* **2004**, *16*, 2918. (c) Yang, C. M.; Lin, H. A.; Zibrowius, B.; Spliethoff, B.; Schüth, F.; Liou, S. C.; Chu, M. W.; Chen, C. H. *Chem. Mater.* **2007**, *19*, 3205.

10.1021/cm800551h CCC: $40.75
Published on Web 10/15/2008

Scheme 1. Schematic Representation of Preparative Steps for the Fe_2O_3@SBA-15 Nanocomposite (samples A−E) and Other Mesoporous Materials (F−H) for Cyt-c Adsorption

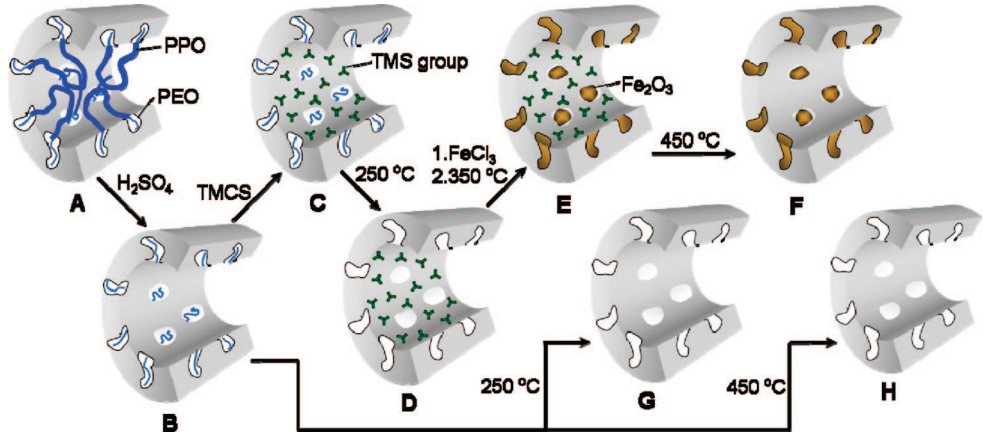

Scheme 1, starting from the selective generation and surface hydrophobization of the mesochannels in SBA-15.[10] The intrawall micropores are then vacated by low-temperature calcination for the deposition of ferric chloride ($FeCl_3$) by simple impregnation. Subsequent heating at 350 °C produces the Fe_2O_3@SBA-15 nanocomposite with Fe_2O_3 nanoparticles in the silica walls, avoiding possible clogging of the mesochannels.[5] Furthermore, the hydrophilic surface of Fe_2O_3 nanoparticles exposed to the open mesochannels, together with the grafted hydrophobic groups, provides unique environment for protein immobilization. In this study, the adsorption of cytochrome c (cyt-c),[11] a small redox metalloprotein with potential for environmental applications,[11e] on Fe_2O_3@SBA-15 has been investigated. Indeed, the magnetically separable Fe_2O_3@SBA-15 nanocomposite exhibits different pH-dependent adsorption behavior and enhanced adsorption capacity, especially at neutral pH, compared to other mesoporous adsorbents.[12,13]

Experimental Section

Synthesis. Mesoporous silica SBA-15 (sample A) was synthesized by adding tetraethoxysilane (TEOS) to the HCl solution of P-123, and the molar composition was 1 TEOS:0.54 HCl:100 H_2O:0.017 P-123.[10b] The mixture was stirred at 35 °C for 24 h, further aged at 60 °C for 24 h, and finally was filtered and dried. One gram of sample A was stirred in 100 mL of 45 wt % H_2SO_4 solution at 95 °C for 20 h, and the product (sample B) was washed and dried at 90 °C. To graft trimethylsilyl (TMS) groups on the exposed surface of sample B, the dried sample was poured in the toluene solution of trimethylchlorosilane (TMCS) and stirred for 1 h, and the product was filtered, washed, and dried (sample C). Further calcination at 250 °C in air for 3 h resulted in sample D. To produce Fe_2O_3@SBA-15 (sample E), 1.0 g of sample D was impregnated with an ethanol solution of 0.68 g of $FeCl_3 \cdot 6H_2O$ and heated at 350 °C in air for 30 min. Three additional samples were prepared for the adsorption studies of cyt-c: sample F was obtained by further heating sample E at 450 °C in air for 3 h to decompose the TMS groups, whereas samples G and H were produced from sample B by further calcination in air at 250 and 450 °C, respectively. The compositions of these samples were studied and confirmed ^{13}C and ^{29}Si NMR spectroscopy and elemental analyses.

Characterizations. Nitrogen physisorption isotherms were measured at 77 K using a Quantachrome Autosorb-1-MP instrument. The isotherms were analyzed by nonlocal density functional theory (NLDFT) method to evaluate pore sizes and micropore volumes of the samples using the kernel of NLDFT equilibrium capillary condensation isotherms of nitrogen at 77 K on silica (adsorption branch, assuming cylindrical pore geometry). The BET surface areas were calculated from the adsorption branches in the relative pressure range of 0.05−0.20, and the total pore volumes were evaluated at a relative pressure of 0.95. Powder X-ray diffraction (PXRD) patterns were obtained on a Mac Science 18MPX diffractometer using Cu Kα radiation. The solid-state NMR spectra were measured on a Bruker DSX400WB spectrometer using 4 mm MAS probes at a spinning rate of 6.5 kHz. Thermalgravimetric (TG) analysis was performed using a Linseis STA PT1600 analyzer. The inductively coupled plasma atomic emission spectroscopy (ICP-AES) data were obtained using a Jarrell-Ash-ICAP 9000 device. Scanning transmission electron microscopy (STEM) and energy-dispersive X-ray spectroscopy (EDX) investigations were performed on a FEI field-emission microscope (Tecnai G^2 F20, operated at 200 kV), and the ultramicrotomed samples with a thickness of about 80−100 nm were prepared for the studies. X-ray absorption spectroscopic (XAS) measurements were performed on the beamline 17C at the National Synchrotron Radiation Research Center (NSRRC), Taiwan. A Quantum Design MPMS-XL7 superconducting quantum interference device (SQUID) magnetometer was used for magnetic characterization. Zeta potential measurements were performed using 90Plus/BI-Zeta Zeta Potential Analyzer (Brookhaven Instruments).

Cyt-c Adsorption Studies. For the cyt-c adsorption experiments, 20 mg of mesoporous adsorbents were suspended in 4 mL of the cyt-c solution with concentrations of cyt-c ranging from 75 to 750 μM, and the mixtures were shaken at 20 °C for 72 h. The cyt-c solutions were prepared by dissolving calculated amounts of cyt-c in 25 mM buffer solutions (citric acid buffer for pH 3.0 and 5.0, potassium phosphate buffer for pH 6.5 and 8.0, sodium bicarbonate buffer for pH 9.6 and 10.6). After centrifugation, the amount of cyt-c in the supernatant liquid was determined by measuring the

(11) (a) Harbury, H. A.; Loach, P. A. *J. Biol. Chem.* **1960**, *235*, 3640. (b) Senn, H.; Wüthrich, K. Q. *Rev. Biophys.* **1985**, *18*, 111. (c) Guo, L. H.; Hill, H. A. O. *Adv. Inorg. Chem.* **1991**, *36*, 341. (d) Macdonald, I. D. G.; Smith, W. E. *Langmuir* **1996**, *12*, 706. (e) Castro, C. E.; Wade, R. S.; Belser, N. O. *Biochem.* **1985**, *24*, 204.
(12) (a) Díaz, J. F.; Balkus, K. J., Jr *J. Mol. Catal. B: Enzymatic* **1996**, *2*, 115. (b) Deere, J.; Magner, E.; Wall, J. G.; Hodnett, B. K. *J. Phys. Chem. B* **2002**, *106*, 7340. (c) Lee, C. H.; Lang, J.; Yen, C. W.; Shih, P. C.; Lin, T. S.; Mou, C. Y. *J. Phys. Chem. B* **2005**, *109*, 12277.
(13) (a) Vinu, A.; Streb, C.; Murugesan, V.; Hartmann, M. *J. Phys. Chem. B* **2003**, *107*, 8297. (b) Vinu, A.; Murugesan, V.; Tangermann, O.; Hartmann, M. *Chem. Mater.* **2004**, *16*, 3056.

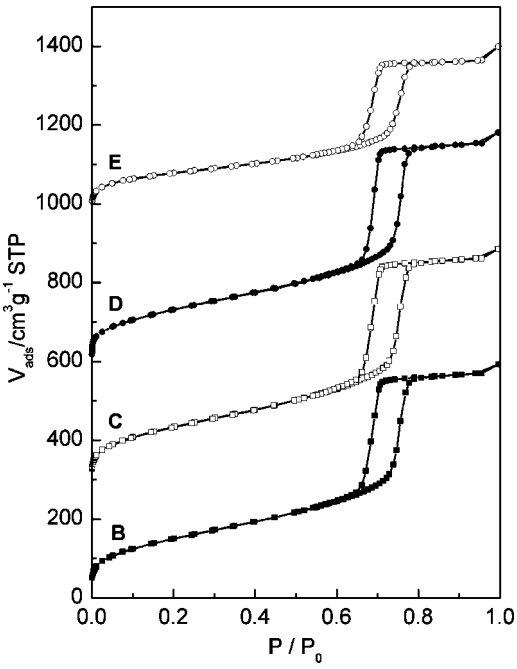

Figure 1. Nitrogen physisorption isotherms of samples B-E referred to Scheme 1. The isotherms are shifted by 280, 560, and 960 cm^3 g^{-1} STP, respectively.

intensity of the 409 nm absorption band (Soret band), from which the adsorbed amount of cyt-c was calculated.

Results and Discussion

The as-synthesized SBA-15 (sample A) exhibits intense (100), (110) and (200) reflections in its small-angle PXRD pattern attributed to an ordered *p6mm* structure.[3] The cell parameter is 11.3 nm, which remains unchanged after the material was subjected to further treatments. Sample A was first treated with H_2SO_4, and the resulting sample B gives a ^{13}C NMR spectrum only with the line attributed to the EO fragments, suggesting a preferential removal of the PO blocks of the P123 copolymers from sample A.[10b] Analysis of the N_2 physisorption isotherm of sample B with a H1-type hysteresis loop, as shown in Figure 1, indicates that the sample has uniform and open mesochannels (7.6 nm in diameter) but very small micropore volume (0.05 cm^3 g^{-1}).

Sample B was then reacted with TMCS to hydrophobize the exposed mesochannel surface and the external surface,[10c] which was confirmed by the appearance of the corresponding lines of the grafted TMS groups in the ^{13}C and ^{29}Si NMR spectra of the resulting sample C. The ^{29}Si NMR spectrum in Figure 2 shows that the grafting leads to a reduction in the relative intensities of the Q^2 and Q^3 lines (Q^n: $Si(OSi)_n(OH)_{4-n}$, $n = 2,3,4$). The intensity ratio (T/Q) of TMS line to Q^n lines is 10.5:100, suggesting that about 27% of the silanol groups in sample B were reacted with TMCS. The grafted TMS groups had little influence on the N_2 sorption isotherm of sample C (see Figure 1), probably because of their small size, and the pore diameter is identical to that for sample B. Further heating sample C at 250 °C caused a selective decomposition of the occluded EO fragments without decomposing the TMS groups, and the resulting sample D possesses large micropore volume of 0.22 cm^3 g^{-1}.

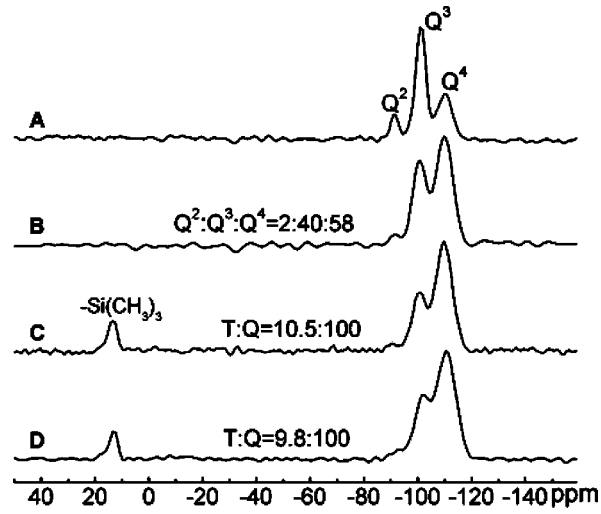

Figure 2. ^{29}Si MAS NMR spectra of samples A−D referred to Scheme 1.

Table 1. Structural Properties of Samples B−H[a]

sample	a_0 (nm)	D^b (nm)	w (nm)	S_{BET} (m^2 g^{-1})	$V_t{}^c$ (cm^3 g^{-1})	$V_m{}^b$ (cm^3 g^{-1})
B	11.3	7.6	3.7	615	0.91	0.05
C	11.3	7.6	3.7	587	0.89	0.04
D	11.3	7.6	3.7	633	1.04	0.22
E	11.3	7.6	3.7	554	0.72	0.02
F	11.1	7.4	3.7	518	0.69	0.01
G	11.3	7.6	3.7	656	1.08	0.24
H	10.9	6.9	4.0	521	0.84	0.15

[a] a_0, unit-cell parameter; D, mesochannel diameter; w, wall thickness; S_{BET}, BET surface area; V_t, total pore volume; V_m, micropore volume. The samples are referred to Scheme 1. [b] Calculated from the adsorption branch using the NLDFT method. [c] Calculated at $P/P_0 = 0.95$.

The ionic $FeCl_3$ was then filled selectively into the hydrophilic micropores of sample D, and subsequent heating at 350 °C in air decomposed the salt and produced Fe_2O_3 nanoparticles in the resulting nanocomposite Fe_2O_3@SBA-15 (sample E). TG analysis suggested that most of the TMS groups (about 90%) survived the heat treatment. Furthermore, elemental analyses by ICP-AES and EDX indicate an average iron-to-silicon atomic ratio (Fe/Si) of 0.15 in sample E. Interestingly, N_2 physisorption analysis indicates that even with such a high loading amount, the mesochannels in sample E are still open without clogging by Fe_2O_3. On the other hand, the micropore volume is significantly decreased (see Table 1), suggesting that Fe_2O_3 nanoparticles were preferentially deposited in the micropores of SBA-15. This is further corroborated by the Z-contrast STEM images of the sample shown in Figure 3. Figure 3a displays a photograph with low magnification, showing that the iron species are uniformly distributed in the host silica. In addition, the characteristic dark contrast observed in the images along the axis of hexagonally arranged mesochannels (images b and c in Figure 3) suggests that the mesochannels in this sample are empty. The rather inhomogeneous bright spots embedded in the relatively gray contrasts arising from the silica walls could be related to Fe_2O_3 nanoparticles because iron is heavier than other constituent elements. These nanoparticles are very small, with a size of about 2−3 nm estimated from the STEM images. In line with this observation, sample E gives very broad and nearly featureless wide-angle PXRD

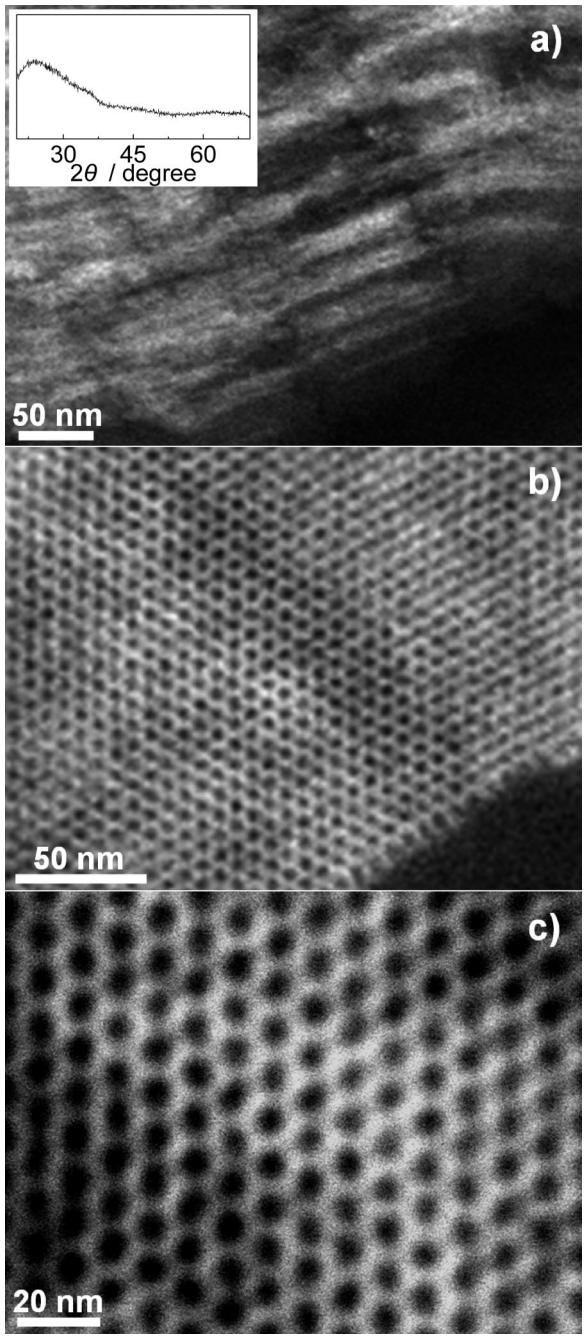

Figure 3. STEM images of sample E viewed (a) perpendicular or (b, c) along the axis of the hexagonally arranged mesopores. The inset in (a) is the wide-angle PXRD pattern of the sample.

pattern (inset in Figure 3a). It should be mentioned that mesoporous aluminosilicates with Fe_2O_3 particles embedded in the walls have been prepared by using specially synthesized poly(isoprene-block-ethylene oxide) copolymers as the structure-directing agent.[14] The embedded iron oxide particles in the resulting materials were larger (~5.6 nm) than those in Fe_2O_3@SBA-15 prepared in this study.

XAS measurements at the Fe K-edge were carried out to obtain structural information on the iron coordination in the Fe_2O_3@SBA-15 nanocomposite. Figure 4a compares the normalized X-ray absorption near-edge structure (XANES)

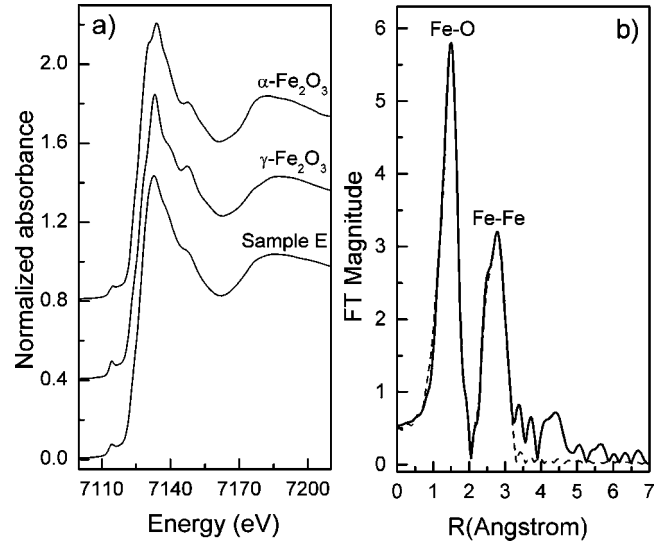

Figure 4. (a) Normalized Fe K-edge XANES spectra of sample E and reference samples. (b) Fourier transform of the k^3-weighted EXAFS and the fit result (dotted line) of sample E.

spectra of sample E and α-Fe_2O_3 and γ-Fe_2O_3 reference samples. The same absorption edge positions for the three samples indicate that the iron ions in sample E are in the +3 oxidation state instead of the +2 oxidation state as in the FeO and Fe_3O_4 reference samples (see Figure S1 in the Supporting Information), whereas the pronounced pre-edge peak for sample E may be correlated to the existence of the tetrahedrally coordinated iron species. In addition, the spectrum for sample E does not resemble either of the spectra for the reference samples; instead, it could be simulated by linear combination of them.[15] Semiquantitative analysis of the edge spectra by the least-squares fitting of linear combinations of spectra of reference samples to the spectrum of the sample gives a rough estimation of 67% α-phase and 33% γ-phase for the iron oxides in Fe_2O_3@SBA-15. The Fourier transform profile of the k^3-weighted extended X-ray absorption fine structure (EXAFS) of sample E, shown in Figure 4b, indicates only the Fe−O and Fe−Fe coordination shells up to 3.5 Å. The best fit bond lengths (R) and corresponding coordination numbers (N) for the Fe−O shell are $R = 1.94$ Å ($N = 2.46$) and 2.11 Å ($N = 0.99$); and for the Fe−Fe shell, $R = 3.01$ Å ($N = 1.36$) and 3.35 Å ($N = 1.43$). The bond lengths are comparable with the fitted results for bulk α-Fe_2O_3 and γ-Fe_2O_3,[16] and the small coordination numbers as well as the significantly reduced magnitude of the FT peaks may be attributed to the small particle sizes with an increased structural disorder for the iron oxides in Fe_2O_3@SBA-15.

The magnetic properties of Fe_2O_3@SBA-15 were investigated by SQUID. Figure 5a shows the temperature dependence of zero-field-cooled (ZFC) and field-cooled (FC) magnetization measured at an applied field of 100 Oe. The ZFC curve presents a peak at a temperature of 82 K which is usually identified as the superparamagnetic blocking

(14) Garcia, C.; Zhang, Y.; DiSalvo, F.; Wiesner, U. *Angew. Chem., Int. Ed.* **2003**, *42*, 1526.

(15) Hsiao, M. C.; Wang, H. P.; Huang, C. H.; Chang, J. E.; Wei, Y. L. *J. Electron Spectrosc. Relat. Phenom.* **2007**, *156−158*, 208.

(16) (a) Fröba, M.; Köhn, R.; Bouffaud, G. *Chem. Mater.* **1999**, *11*, 2858. (b) Corrias, A.; Ennas, G.; Mountjoy, G.; Paschina, G. *Phys. Chem. Chem. Phys.* **2000**, *2*, 1045.

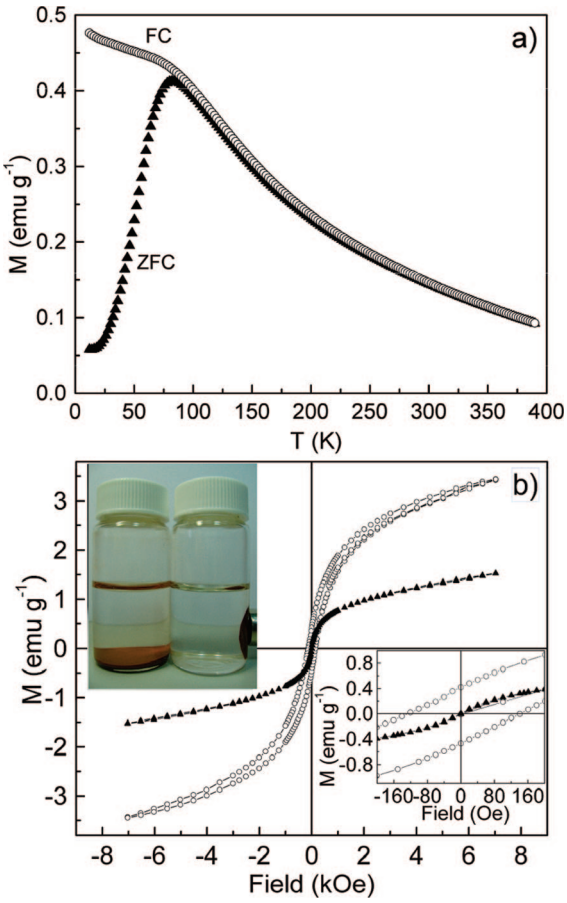

Figure 5. (a) ZFC and FC (100 Oe) magnetization curves for sample E. (b) Field-dependent magnetization of sample E measured at 300 K (▲) and 2 K (○). The insets are the magnification near the origin (lower right) and a photograph showing magnetic capture of sample E (upper left).

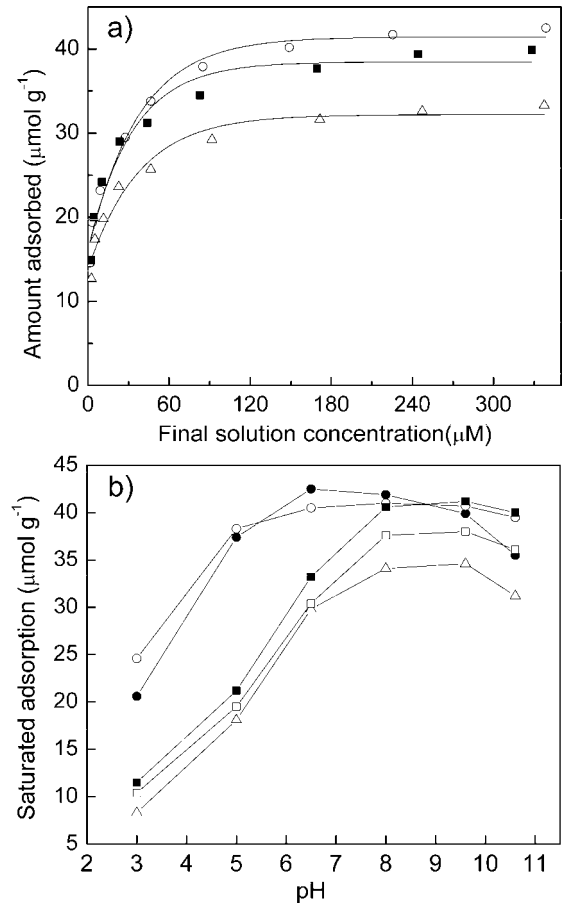

Figure 6. (a) Adsorption isotherms at 20 °C of cyt-c on sample E at solution pH of 6.5 (○), 9.6 (■), and 10.6 (Δ). (b) The pH dependence of the saturated adsorptions for samples D (○), E (●), F (Δ), G (■), and H (□) referred to Scheme 1.

temperature (T_b).[14,17] Above T_b, ZFC and FC curves coincide and are inversely proportional to temperature. The field-dependent magnetization (Figure 5b) also confirms the superparamagnetism of the sample:[18] It exhibits no hysteresis at 300 K but becomes hysteretic at 2 K, a temperature far below T_b. The coercivity field and the remnant magnetization at 2 K are 140 Oe and 0.44 emu g^{-1}, respectively. The saturation magnetizations (σ_s) are 1.5 emu g^{-1} at 300 K and 3.5 emu g^{-1} at 2 K, which correspond to the values of 15.7 emu (at 300 K) and 36.9 emu (at 2 K) per gram of γ-Fe_2O_3, assuming that 33% of the iron oxides are in the γ-phase. The σ_s values are considerably smaller than that of bulk γ-Fe_2O_3 ($\sigma_s = 76$ emu g^{-1}), which may be attributed to the presence of magnetically inactive layers at the surface of small γ-Fe_2O_3 nanoparticles.[17b,19] In addition, the fact that the hysteresis loop of the magnetization curve at 2 K is open up to large field could be associated with the surface effects for very small magnetic nanoparticles.[18b,20]

The magnetically separable Fe_2O_3@SBA-15 nanocomposite has fully open mesochannels and bifunctional surface of the hydrophobic TMS groups and the exposed Fe_2O_3 nanoparticles, and its application for the adsorption of the horse heart cyt-c at different solution pHs was studied. As shown in Figure 6a, each adsorption isotherm exhibits a sharp initial rise and reaches a plateau at high protein concentrations, suggesting that the affinity between cyt-c and the adsorbent surface is high and the adsorption follows a simple Langmuir model.[13] On the other hand, Fe_2O_3@SBA-15 (sample E) exhibits maximal adsorption of cyt-c at around pH 6.5−8.0 (Figure 6b), which is distinct from other reported mesoporous adsorbents[13] showing maximal adsorptions at a pH (pH 9.6) close to the isoelectric point of cyt-c (IEP_{cyt}, about 9.8).[11d] The finding is interesting since the structural stability and redox properties of cyt-c are known to be associated to the solution pH,[9c,21] and adsorbents with high cyt-c uptake at neutral (or physiological) pH are usually preferred for applications.[11e]

(17) (a) Park, J.; An, K.; Hwang, Y.; Park, J. G.; Noh, H. J.; Kim, J. Y.; Park, J. H.; Hwang, N. M.; Hyeon, T. *Nat. Mater.* **2004**, *3*, 891. (b) Long, J. W.; Logan, M. S.; Rhodes, C. P.; Carpenter, E. E.; Stroud, R. M.; Rolison, D. R. *J. Am. Chem. Soc.* **2004**, *126*, 16879.
(18) (a) Yi, D. K.; Lee, S. S.; Papaefthymiou, G. C.; Ying, J. Y. *Chem. Mater.* **2006**, *18*, 614. (b) Delahaye, E.; Escax, V.; El Hassan, N.; Davidson, A.; Aquino, R.; Dupuis, V.; Perzynski, R.; Raikher, Y. L. *J. Phys. Chem. B* **2006**, *110*, 26001.
(19) Berkowitz, A. E.; Schuele, W. J.; Flanders, P. J. *J. Appl. Phys.* **1968**, *39*, 1261.
(20) *Surface Effects in Magnetic Nanoparticles*; Fiorani, D., Ed.; Springer: New York, 2005.
(21) (a) Bowden, E. F.; Hawkridge, F. M.; Blount, H. N. *J. Electroanal. Chem.* **1984**, *161*, 355. (b) Boffi, F.; Bonincontro, A.; Cinelli, S.; Castellano, A. C.; De Francesco, A.; Della Longa, S.; Girasole, M.; Onori, G *Biophys. J.* **2001**, *80*, 1473.

The saturated cyt-c adsorptions as a function of the solution pH for sample D (with grafted TMS groups but no Fe_2O_3), sample F (with intercalated Fe_2O_3 but no TMS groups) and two pure-silica adsorbents (samples G and H, cf. Scheme 1 and Table 1) are also shown in Figure 6b. Samples G and H have similar pH-dependent adsorption capacities for cyt-c as other pure-silica adsorbents,[12a,13b] exhibiting saturated adsorptions peaked at pH 9.6 and decreased dramatically when pH is lower than 8.0. Similar pH-dependency is observed for sample F, but the saturated adsorption is even smaller than the pure-silica adsorbents possibly due to the additional weight of the incorporated Fe_2O_3 in this sample. For sample D, its saturated adsorption is relatively large and does not change too much in the pH range of 6−11. The distinct pH-dependent adsorption profile for this sample may be attributed to the hydrophobic surface of the TMS-grafted mesopores.

The saturated adsorptions of the five adsorbents at pH 6.5 are further compared. The low adsorption capacity for samples F−H at this pH may be mainly attributed to the electrostatic repulsion between the adsorbed cyt-c,[6a,13] which has a inhomogeneous distribution of charged and nonpolar amino acid residues on its surface.[11] For samples D and E, the saturated adsorptions are significantly larger than those for the other three, suggesting that the hydrophobic interactions between the TMS groups on the mesopores and the cyt-c molecules might be dominant over other attractive interactions. On the other hand, although the two samples exhibit similar saturated adsorption values normalized to the total adsorbent weight, the fraction of the mesopore volume occupied by the protein for the two samples are significantly different. On the basis of a dimension of 2.6 nm × 3.2 nm × 3.0 nm for the horse heart cyt-c,[11c] the occupied volumes corresponding to the saturated adsorptions are 0.349 $cm^3\ g^{-1}$ for sample D and 0.366 $cm^3\ g^{-1}$ for sample E. With the mesopore volumes estimated from nitrogen physisorption measurements (cf. Table 1), the volume fractions occupied by cyt-c in samples D and E (Fe_2O_3@SBA-15) are estimated to be 34 and 51%, respectively. A comparison of the values seems to suggest that in addition to the hydrophobic interactions, the surface of Fe_2O_3 nanoparticles also plays a positive role in the adsorption of cyt-c in Fe_2O_3@SBA-15. One of the probable ways for the Fe_2O_3 nanoparticles to contribute to the cyt-c adsorption is through electrostatic interactions with the positively charged cyt-c knowing that the surface properties of iron oxide are strongly associated with the preparation route, crystalline phase, particle size, and the solution conditions (e.g., type and concentration of the electrolytes).[22] Selected samples were further characterized by measuring the zeta potential in the potassium phosphate buffer solution at pH 6.5. It was found that although the zeta potentials for pure-silica adsorbents (samples G and H) were −25 to −30 mV, sample E showed a zeta potential of about −11 mV. Because most of the grafted TMS groups on the mesochannel surface and the external surface in sample E remained intact, as discussed previously, the measured negative potential in the buffered pH 6.5 solution might be mainly attributed from the surface of Fe_2O_3 in Fe_2O_3@SBA-15 although possible contribution from the exposed silica surface could not be fully excluded.

Conclusions

In summary, the Fe_2O_3@SBA-15 nanocomposite with superparamagnetic properties, fully open mesochannels and bifunctional surface properties has been prepared. By selectively hydrophobizing the mesopore surface of SBA-15, ionic iron salt can be selectively deposited into the micropores and, upon further heat treatment in air, transformed into oxide nanoparticles in the micropores. The unique bifunctional surface of the Fe_2O_3@SBA-15 nanocomposite has been found to enhance the adsorption capacity for cytochrome c. In addition, the fact that Fe_2O_3@SBA-15 exhibits maximum saturated uptake at neutral solution pH makes the nanocomposite potentially useful for practical applications when neutral or physiological pH environment is required.

Acknowledgment. The authors thank Mr. Shih-Chi Wang and Professor Yu Wang for the SQUID measurements and the National Science Council of the Republic of China for financial support under Contracts NSC95-2113-M-007-032-MY and NSC95-2911-I-007-030.

Supporting Information Available: The Fe K-edge XANES spectra of four reference samples. This material is available free of charge via the Internet at http://pubs.acs.org.

CM800551H

(22) Kosmulski, M. In *Chemical Properties of Material Surfaces*; Hubbard, A. T., Ed.;Surfactant Science Series; Marcel Dekker: New York, 2001; Vol. 102, pp 65−309.